eLIFE
elifesciences.org

Figures and figure supplements

Optimal multisensory decision-making in a reaction-time task

Jan Drugowitsch, et al.

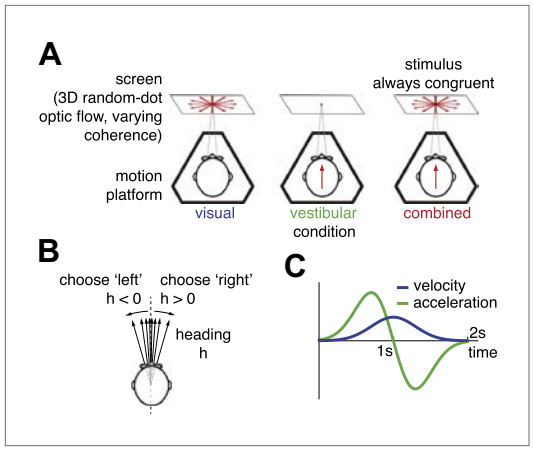

Figure 1. Heading discrimination task. (**A**) Subjects are seated on a motion platform in front of a screen displaying 3D optic flow. They perform a heading discrimination task based on optic flow (visual condition), platform motion (vestibular condition), or both cues in combination (combined condition). Coherence of the optic flow is constant within a trial but varies randomly across trials. (**B**) The subjects' task is to indicate whether they are moving rightward or leftward relative to straight ahead. Both motion direction (sign of *h*) and heading angle (magnitude of |*h*|) are chosen randomly between trials. (**C**) The velocity profile is Gaussian with peak velocity ~1 s after stimulus onset.
DOI: 10.7554/eLife.03005.003

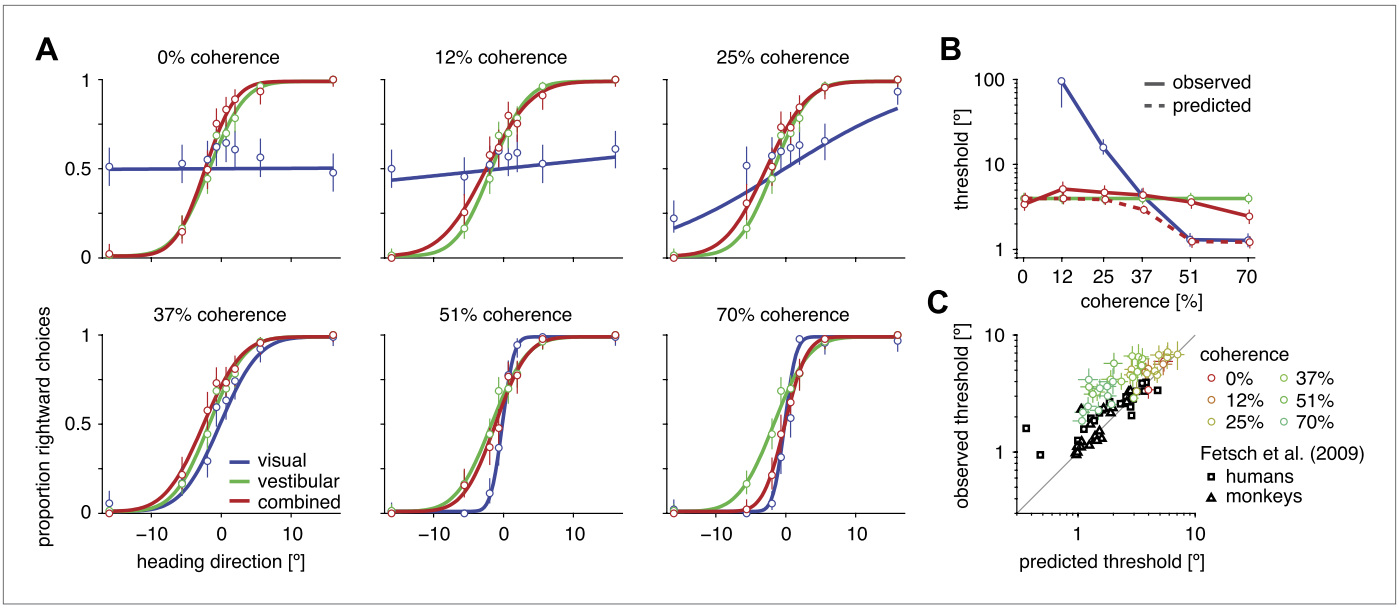

Figure 2. Heading discrimination performance. (**A**) Plots show the proportion of rightward choices for each heading and stimulus condition. Data are shown for subject D2, who was tested with 6 coherence levels. Error bars indicate 95% confidence intervals. (**B**) Discrimination threshold for each coherence and condition for subject D2 (see ***Figure 2—figure supplement 1*** for discrimination thresholds of all subjects). For large coherences, the threshold in the combined condition (solid red curve) lies between that of the vestibular and visual conditions, a marked deviation from the standard prediction (dashed red curve) of optimal cue integration theory. (**C**) Observed vs predicted discrimination thresholds for the combined condition for all subjects. Data are color coded by motion coherence. Error bars indicate 95% CIs. For most subjects, observed thresholds are significantly greater than predicted, especially for coherences greater than 25%. For comparison, analogous data from monkeys and humans (black triangles and squares, respectively) are shown from a previous study involving a fixed-duration version of the same task (***Fetsch et al., 2009***).

DOI: 10.7554/eLife.03005.004

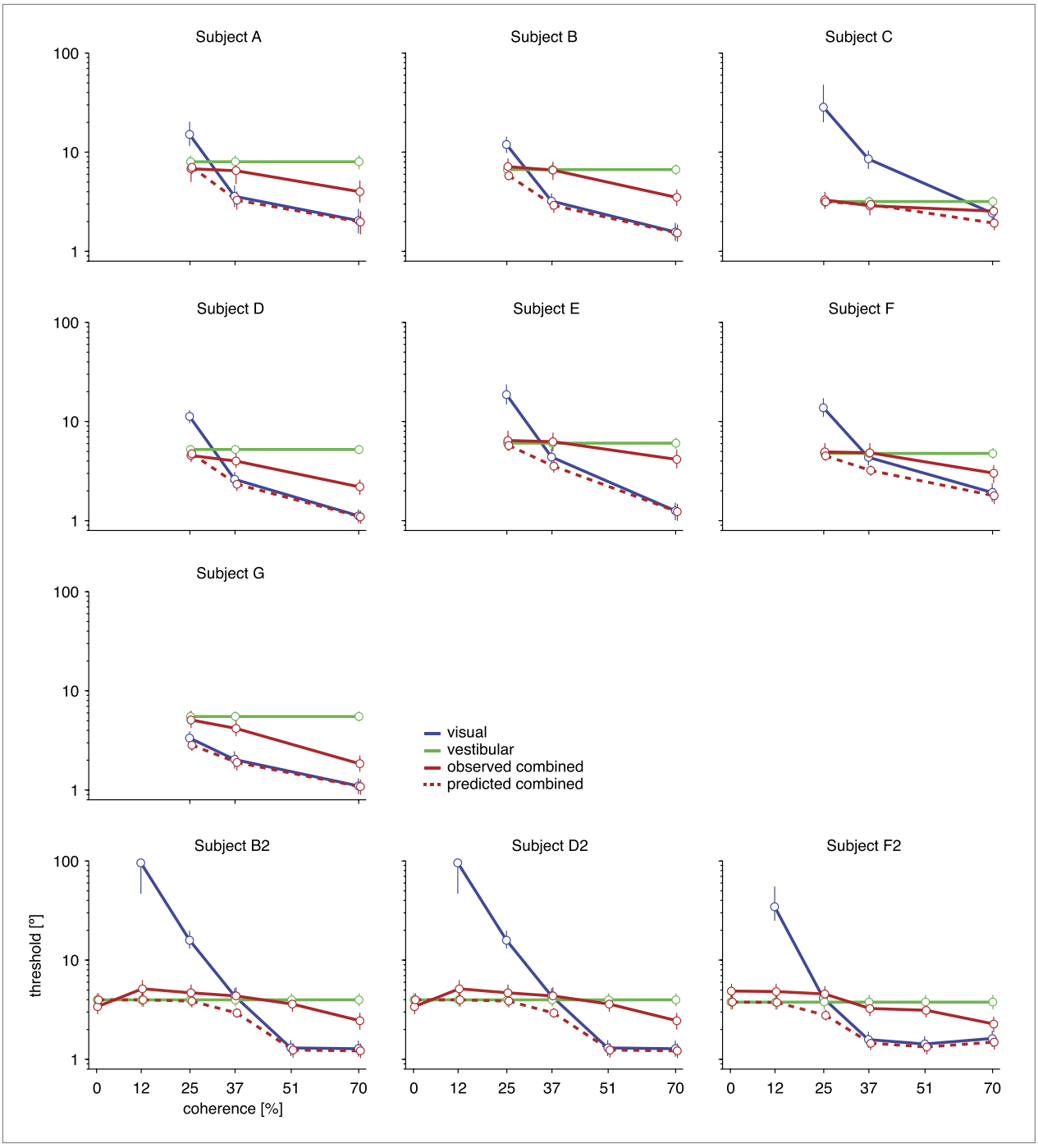

Figure 2—figure supplement 1. Discrimination thresholds for all subjects and conditions.
DOI: 10.7554/eLife.03005.005

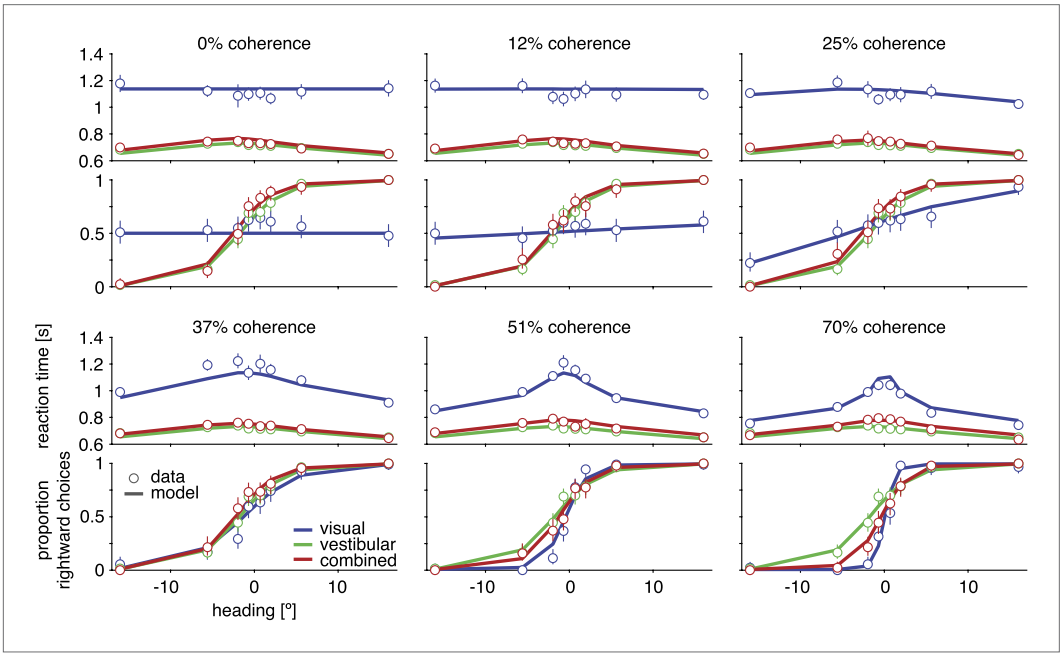

Figure 3. Discrimination performance and reaction times for subject D2. Behavioral data (symbols with error bars) and model fits (lines) are shown separately for each motion coherence. Top plot: reaction times as a function of heading; bottom plot: proportion of rightward choices as a function of heading. Mean reaction times are shown for correct trials, with error bars representing two SEM (in some cases smaller than the symbols). Error bars on the proportion rightward choice data are 95% confidence intervals. Although reaction times are only shown for correct trials, the model is fit to data from both correct and incorrect trials. See ***Figure 3—figure supplement 1*** for behavioral data and model fits for all subjects. ***Figure 3—figure supplement 2*** shows the fitted model parameters per subject.

DOI: 10.7554/eLife.03005.006

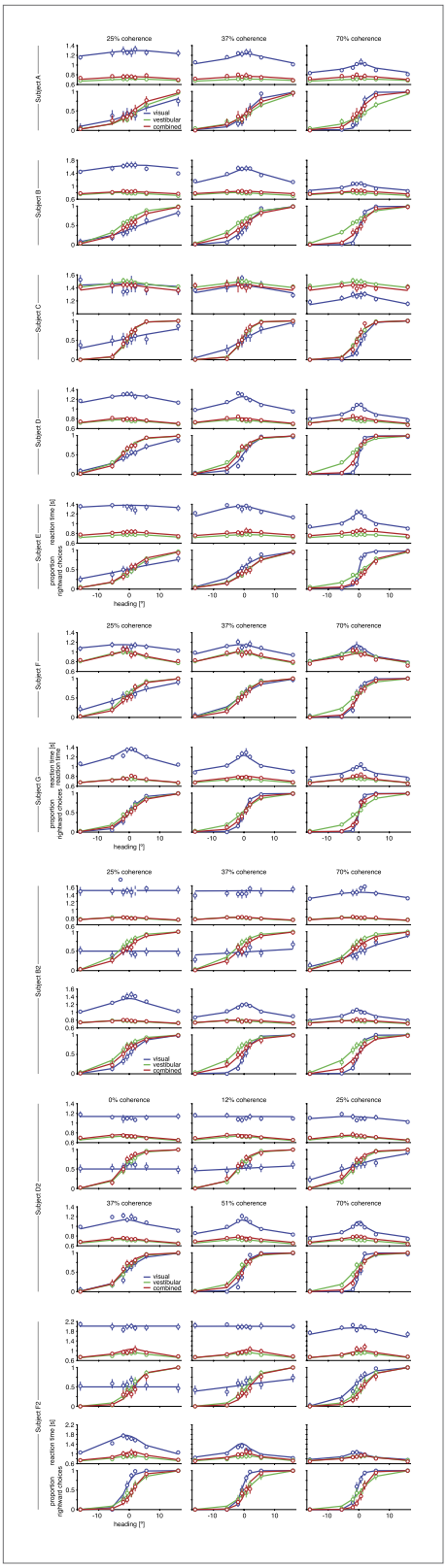

Figure 3—figure supplement 1. Psychometric functions, chronometric functions, and model fits for all subjects.
DOI: 10.7554/eLife.03005.007

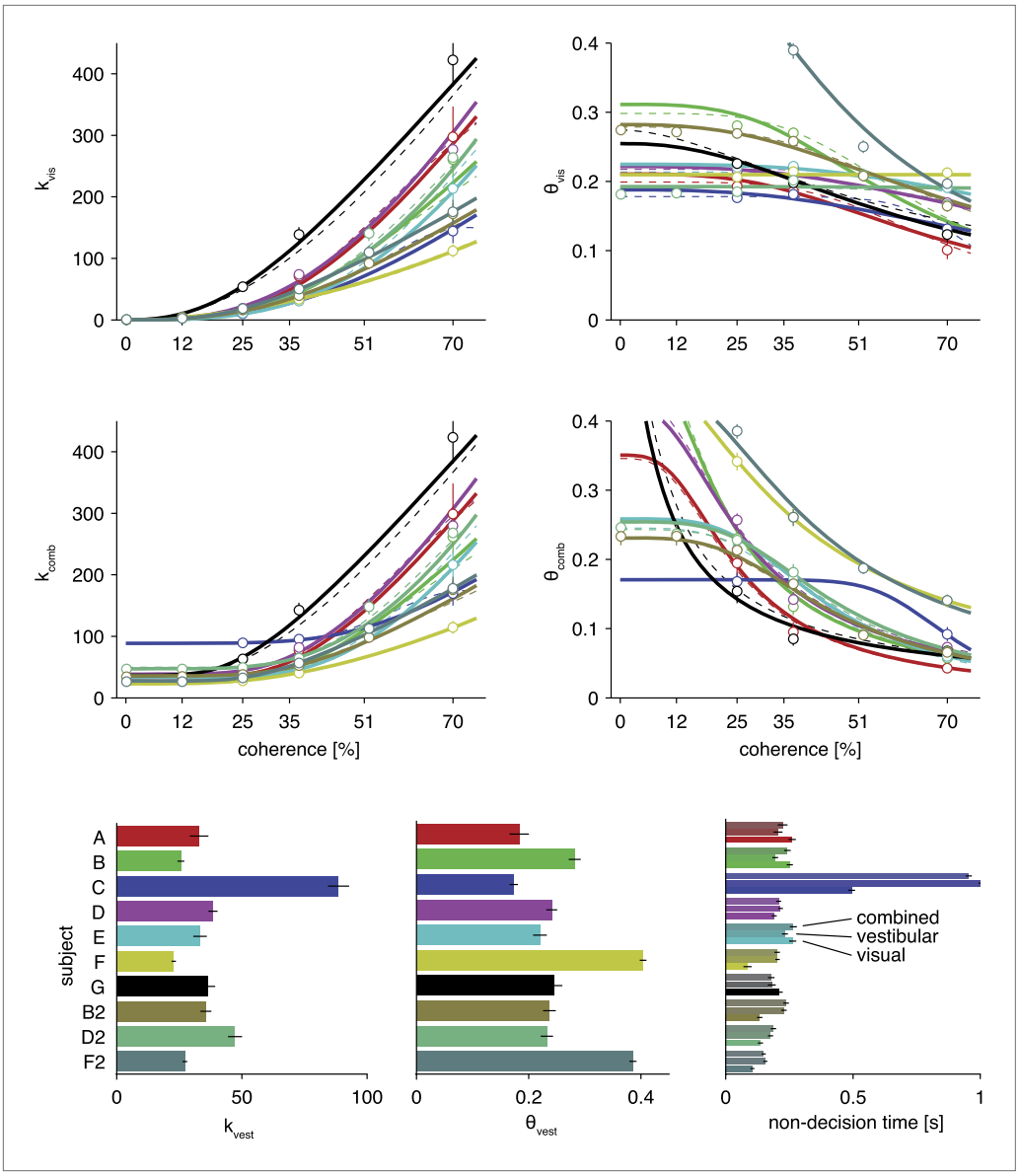

Figure 3—figure supplement 2. Model parameters for fits of the optimal model and two alternative parameterizations.

DOI: 10.7554/eLife.03005.008

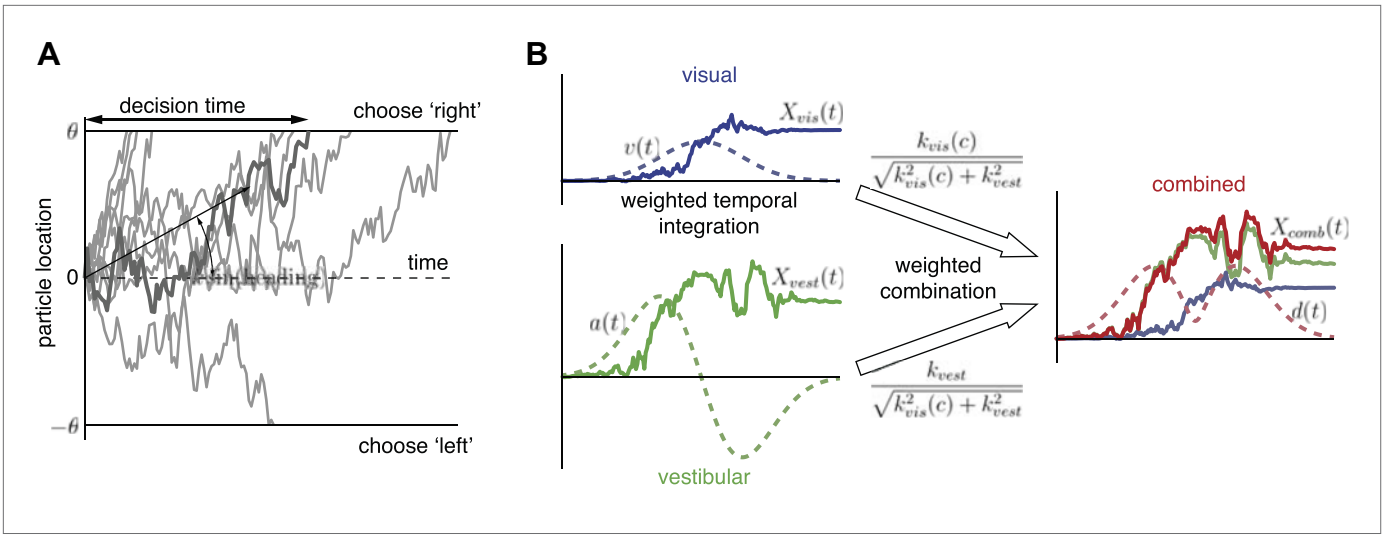

Figure 4. Extended diffusion model (DM) for heading discrimination task. (**A**) A drifting particle diffuses until it hits the lower or upper bound, corresponding to choosing 'left' or 'right' respectively. The rate of drift (black arrow) is determined by heading direction. The time at which a bound is hit corresponds to the decision time. 10 particle traces are shown for the same drift rate, corresponding to one incorrect and nine correct decisions. (**B**) Despite time-varying cue sensitivity, optimal temporal integration of evidence in DMs is preserved by weighting the evidence by the momentary measure of its sensitivity. The DM representing the combined condition is formed by an optimal sensitivity-weighted combination of the DMs of the unimodal conditions.

DOI: 10.7554/eLife.03005.009

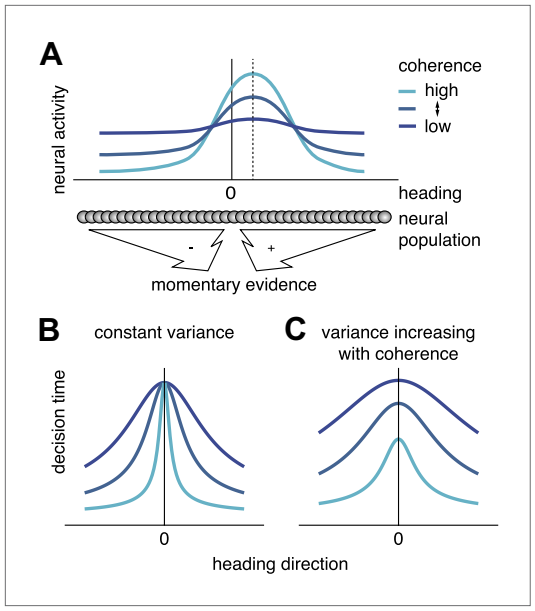

Figure 5. Scaling of momentary evidence statistics of the diffusion model (DM) with coherence. (**A**) Assumed neural population activity giving rise to the DM mean and variance of the momentary evidence, and their dependence on coherence. Each curve represents the activity of a population of neurons with a range of heading preferences, in response to optic flow with a particular coherence and a heading indicated by the dashed vertical line. (**B**) Expected pattern of reaction times if variance is independent of coherence. If neither the DM bound nor the DM variance depend on coherence, the DM predicts the same decision time for all small headings, regardless of coherence. This is due to the DM drift rate, $k_{vis}(c)sin(h)$ being close to 0 for small headings, $h \approx 0$, independent of the DM sensitivity $k_{vis}(c)$. (**C**) Expected pattern of reaction times when variance scales with coherence. If both DM sensitivity and DM variance scale with coherence while the bound remains constant, the DM predicts different decision times across coherences, even for small headings. Greater coherence causes an increase in variance, which in turn causes the bound to be reached more quickly for higher coherences, even if the heading, and thus the drift rate, is small.

DOI: 10.7554/eLife.03005.010

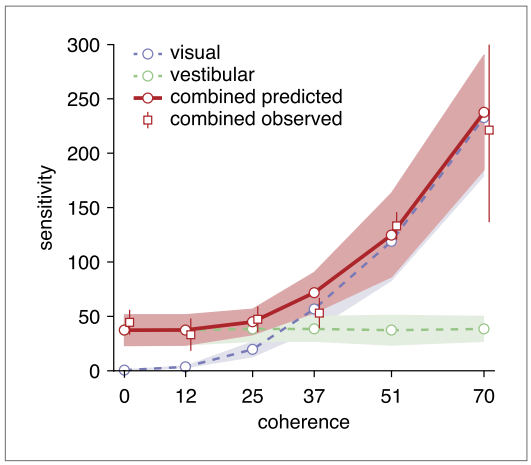

Figure 6. Predicted and observed sensitivity in the combined condition. The sensitivity parameter measures how sensitive subjects are to a change of heading. The solid red line shows predicted sensitivity for the combined condition, as computed from the sensitivities of the unimodal conditions (dashed lines). The combined sensitivity measured by fitting the model to each coherence separately (red squares) does not differ significantly from the optimal prediction, providing strong support to the hypothesis that subjects accumulate evidence near-optimally across time and cues. Data are averaged across datasets (except 0%, 12%, 51% coherence: only datasets B2, D2, F2), with shaded areas and error bars showing the 95% CIs.
DOI: 10.7554/eLife.03005.011

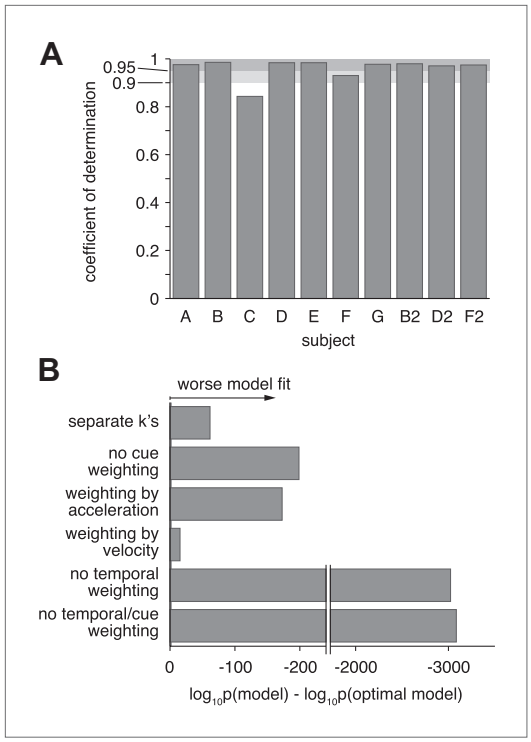

Figure 7. Model goodness-of-fit and comparison to alternative models. (**A**) Coefficient of determination (adjusted R^2) of the model fit for each of the ten datasets. (**B**) Bayes factor of alternative models compared to the optimal model. The abscissa shows the base-10 logarithm of the Bayes factor of the alterative models vs the optimal model (negative values mean that the optimal model out-performs the alternative model). The gray vertical line close to the origin (at a value of −2 on the abscissa) marks the point at which the optimal model is 100 times more likely than each alternative, at which point the difference is considered 'decisive' (***Jeffreys, 1998***). Only the 'separate k's' model has more parameters than the optimal model, but the Bayes factor indicates that the slight increase in goodness-of-fit does not justify the increased degrees of freedom. The 'no cue weighting' model assumes that visual and vestibular cues are weighted equally, independent of their sensitivities. The 'weighting by acceleration' and 'weighting by velocity' models assume that the momentary evidence of both cues is weighted by the acceleration and velocity profile of the stimulus, respectively. The 'no temporal weighting' model assumes that the evidence is not weighted over time according to its sensitivity. The 'no cue/temporal weighting' model lacks both weighting of cues by sensitivity and weighting by temporal profile. All of the tested alternative models explain the data decisively worse than the optimal model. ***Figure 7—figure supplement 1*** shows how individual subjects contribute to this model comparison, and the results of a more conservative Bayesian random-effects model comparison that supports same conclusion. ***Figure 7—figure supplement 2*** compares the proposed model to ones with alternative parameterizations.

DOI: 10.7554/eLife.03005.012

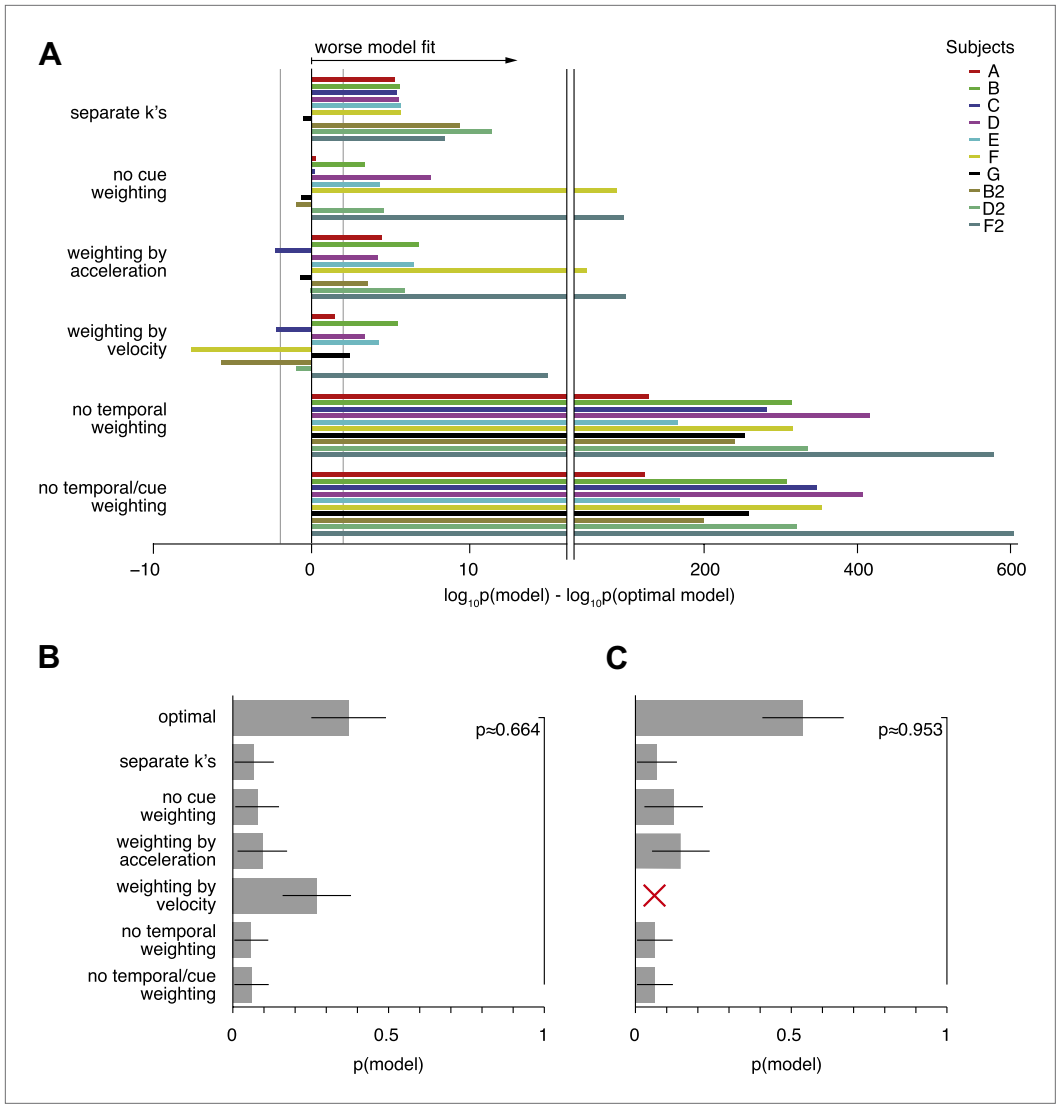

Figure 7—figure supplement 1. Model comparison per subject, and random-effects model comparison.
DOI: 10.7554/eLife.03005.013

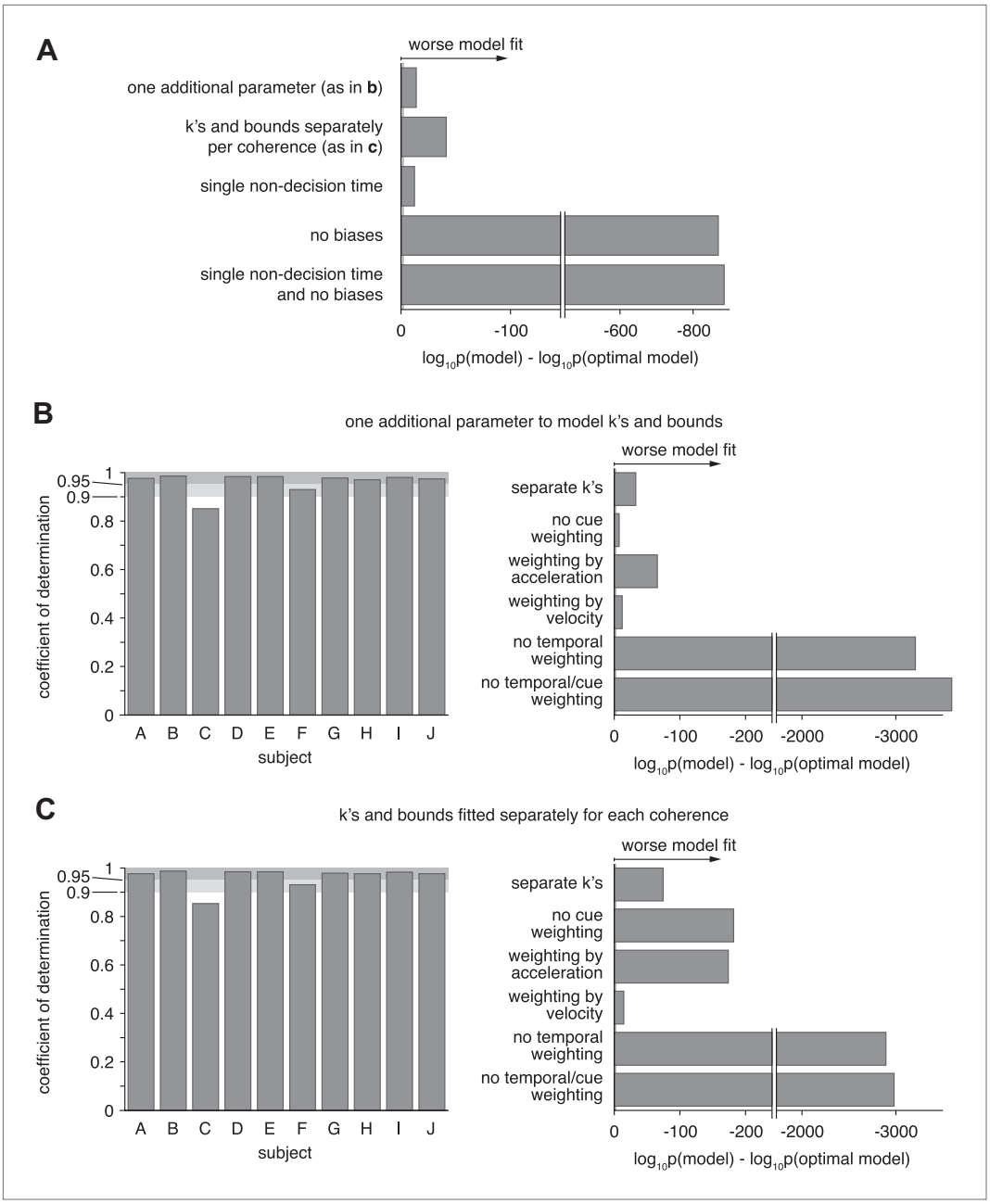

Figure 7—figure supplement 2. Model comparison for models with alternative parameterization.
DOI: 10.7554/eLife.03005.014